APPENDIX C

Hydrodynamic Modeling Report

ERDC/CHL LETTER REPORT

Coastal and Hydraulics Laboratory

US Army Corps
of Engineers®
Engineer Research and
Development Center

Hydrodynamic, Wave and Sediment Transport Modeling around Third Port in Skiffes Creek and James River

Honghai Li, Holly N. Berckenhoff, Joseph W. McMahon, and Megan A. Wood

November 2021

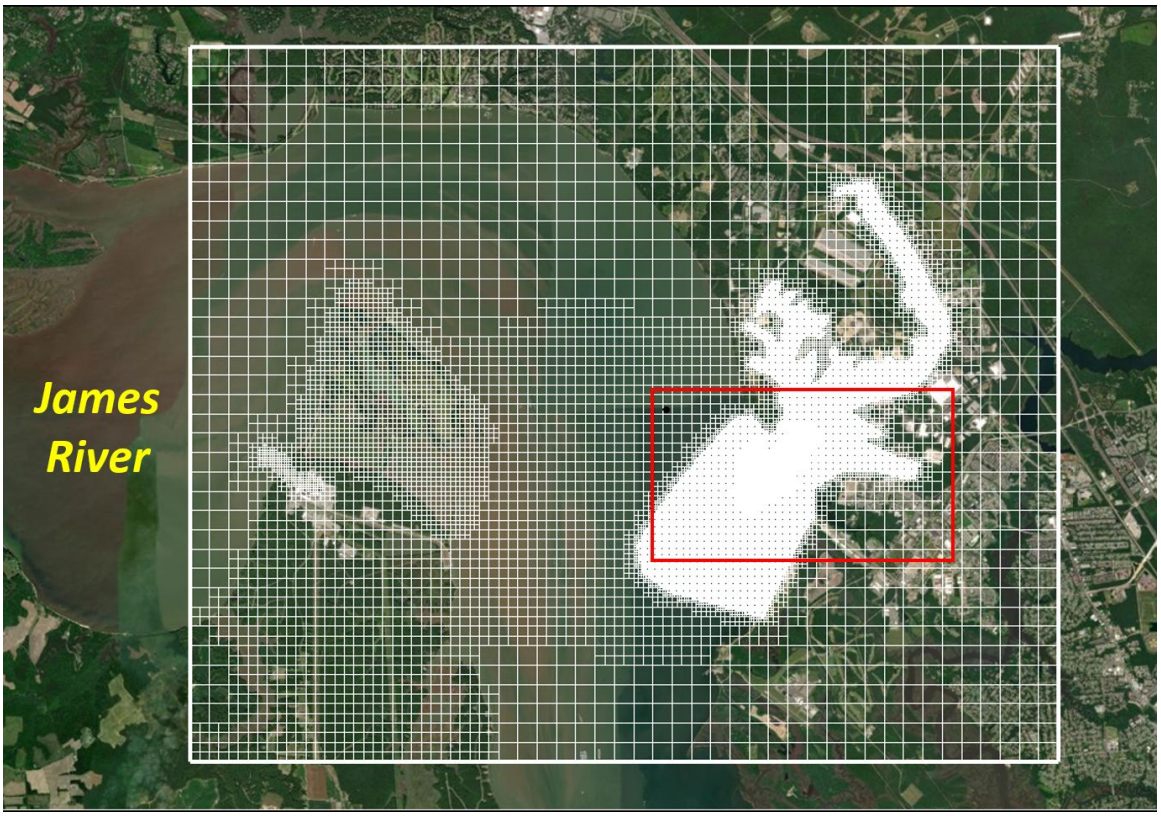

ERDC/CHL LETTER REPORT
November 2021

Hydrodynamic, Wave and Sediment Transport Modeling around Third Port in Skiffes Creek and James River

Honghai Li

Coastal and Hydraulics Laboratory
U.S. Army Engineer Research and Development Center
3909 Halls Ferry Road
Vicksburg, MS 39180-6199

Holly N. Berckenhoff, Joseph W. McMahon, and Megan A. Wood

U.S. Army Corps of Engineers
Norfolk District
803 Front Street
Norfolk, VA 23510

Letter Report

Prepared for U.S. Army Engineer District, Norfolk
803 Front Street
Norfolk, VA 23510

Table of Contents

Figures and Tables

Figures

Tables

Preface

This study was conducted for the U.S. Army Engineer District, Norfolk (NAO) by the Coastal and Hydraulics Laboratory (CHL) of the US Army Engineer Research and Development Center (ERDC), funding provided by NAO.

This work was conducted under the general administrative supervision of Ms. Lauren M. Dunkin, Chief of Coastal Engineering Branch, and Ms. Ashley Frey, Chief of the Navigation Division. Mr. Ketth Flowers and Dr. Ty V. Wamsley were the Deputy and Director of CHL during this study period, respectively.

At the time of publication of this report, COL Teresa A. Schlosser was Commander and Executive Director of ERDC. Dr. David W. Pittman was ERDC Director.

Unit Conversion Factors

Multiply	By	To Obtain
cubic yards	0.7645549	cubic meters
Feet	0.3048	meters
Yards	0.9144	meters

1 Introduction

The Third Port is located at the northwest corner of Newport News, Virginia, and at the confluence of Skiffes Creek and the James River (Figure 1). The port includes a fleet of vessels and tugboats, the land ship facility, a modular causeway mooring area, and a boat ramp. The modular causeway mooring field is located at the north side of the port and is oriented from southwest to northeast, spanning a length of approximately 300 m from the James River into Skiffes Creek. Due to lack of fendering, mooring dolphins along the field have been deteriorating throughout the years. Additionally, the mooring area was proposed to be relocated further upstream along the navigation channel to maximize the usable waterway. To reduce sedimentation, allow future maintenance dredging, and mitigate the potential for impacts on the wetland adjacent to the mooring area, the relocation of the current mooring field with the construction of an underwater bulkhead or revetment was proposed (McLaren Engineering Group 2019). (Figure 1).

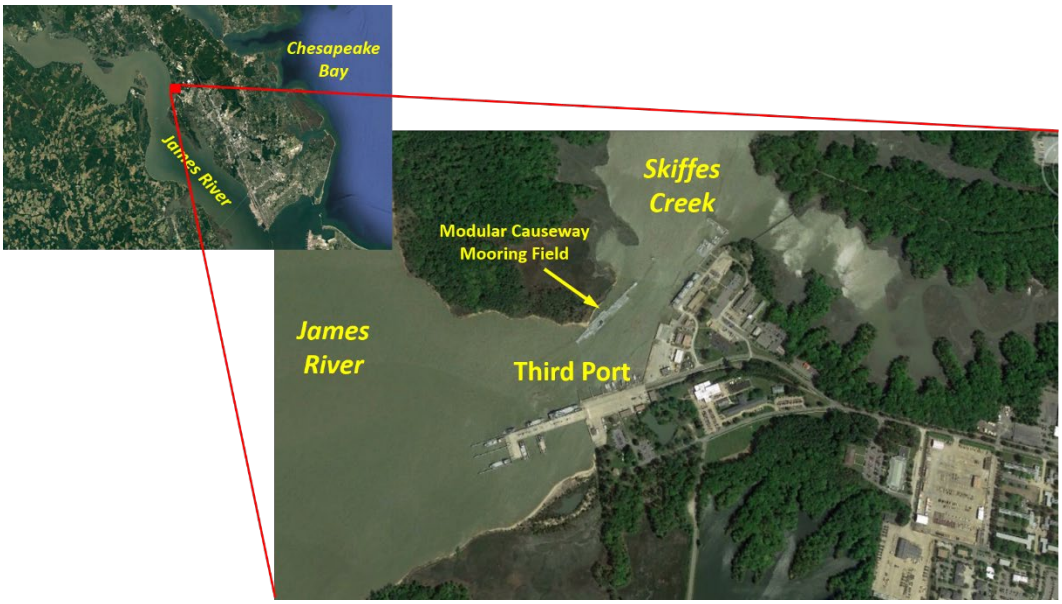

Figure 1. Study site around the Third Port.

Facing north-northwest with James River on its west, the port gets frequent wave impact from extratropical storms. To reduce incident wave energy and protect the port from wave damage, proposed modifications to the current piers and the designing and the addition of a wave screen are in planning. For rigorous evaluation of the project impacts on the local environment,

mathematical modeling on hydrodynamics, waves, and sediment transport needs to be carried out and coastal engineering analyses to be conducted.

Hydrodynamic, wave, and sediment transport modeling for the Third Port at Fort Eustis was conducted using the Coastal Modeling System (CMS). The CMS is an integrated suite of numerical models, consisting of a hydrodynamic and sediment transport model, CMS-Flow, and a spectral wave transformation model, CMS-Wave. The coupled modeling system calculates time-dependent water surface elevation, current, waves, sediment transport, and morphology change in coastal ocean, estuarine, and lake applications.

CMS-Flow is a two-dimensional (2-D) finite-volume model that solves the mass conservation and shallow-water momentum equations of water motion on a non-uniform Cartesian grid (Sanchez et al., 2011a, b). Wave radiation stresses and wave parameters are calculated by CMS-Wave and supplied to CMS-Flow for the flow and sediment transport calculations.

CMS-Wave is a 2-D spectral wave transformation model that solves the steady-state wave-action balance equation on a non-uniform Cartesian grid (Lin et al., 2008). The model is designed to simulate wave processes that are significant in coastal zones, in the vicinity of jetties and breakwaters, and in ports and harbors. These processes include wave shoaling, refraction, diffraction, reflection, wave breaking and dissipation, wave runup and overtopping, wave-structure and wave-current interactions, and wave generation and growth mechanisms. Water level, current, and morphology changes calculated by CMS-Flow are provided to CMS-Wave at user-specified intervals to complete the coupling between CMS-Flow and CMS-Wave, which are operated through the surface-water modeling system (SMS) (Aquaveo, 2020). The framework of CMS is shown in Figure 2.

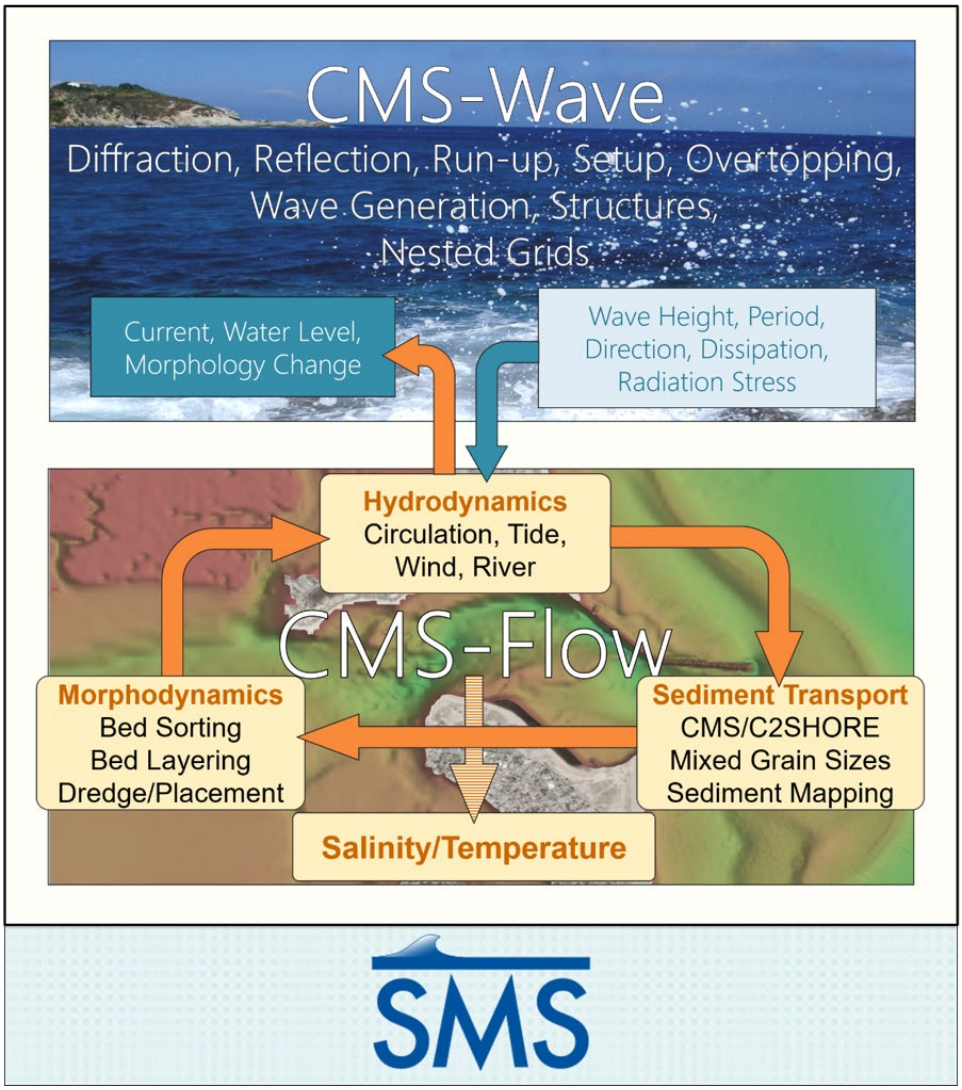

Figure 2. The CMS framework and its components.

For this application, the CMS is driven by water levels and winds. The current and wave conditions are calculated to investigate sediment movement, bed volume change, and wave propagation around the Third Port.

2 Model Setup

CMS-Flow domain is discretized by a telescoping grid, which is 14.5 km in the east-west direction and 12.0 km in the north-south direction. The telescoping grid has approximately 48,000 computational cells. The fine resolution cells with 10-20 m spacing are specified around the Third Port and the harbor channel and the coarse resolution with 320-m spacing in James River boundaries. The average water depth is 2.8 m around the port and 5.3 m within the navigation channel (Figure 3).

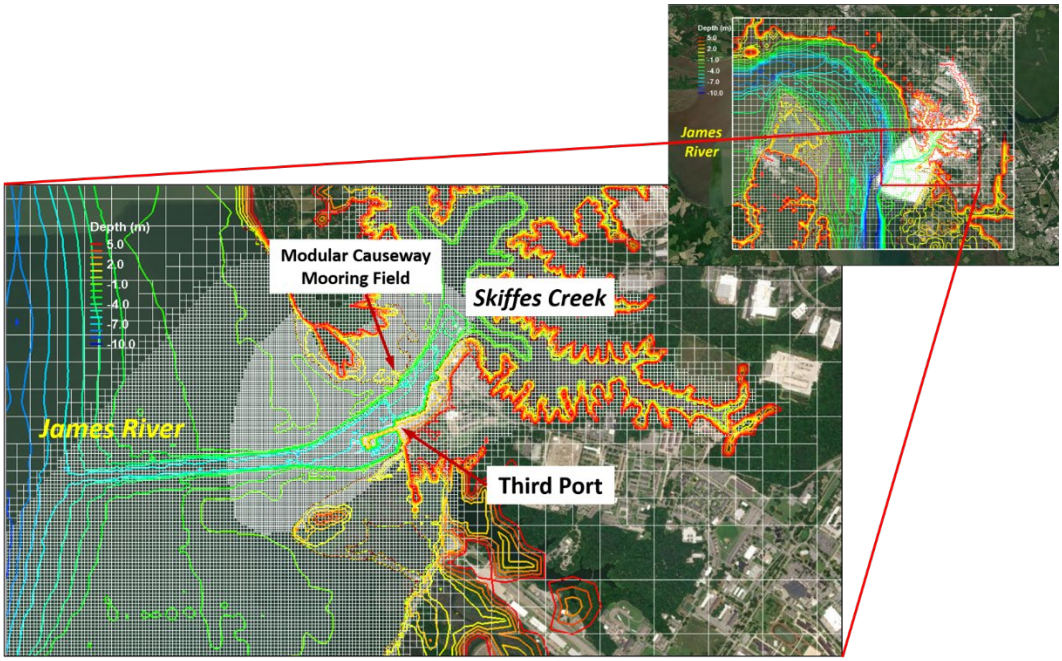

Figure 3. CMS domain, CMS-Flow telescoping grid and bathymetry.

CMS-Wave domain is within the CMS-Flow domain with a horizontal scale of 11.4 ×11.7 km (Figure 4). Non-uniform rectangular grid is used for the wave model. Similar to the discretization of the flow model, high resolution grids of 10.0 × 10.0 m are specified around the port and grid cell sizes increase to 300 m away from the port.

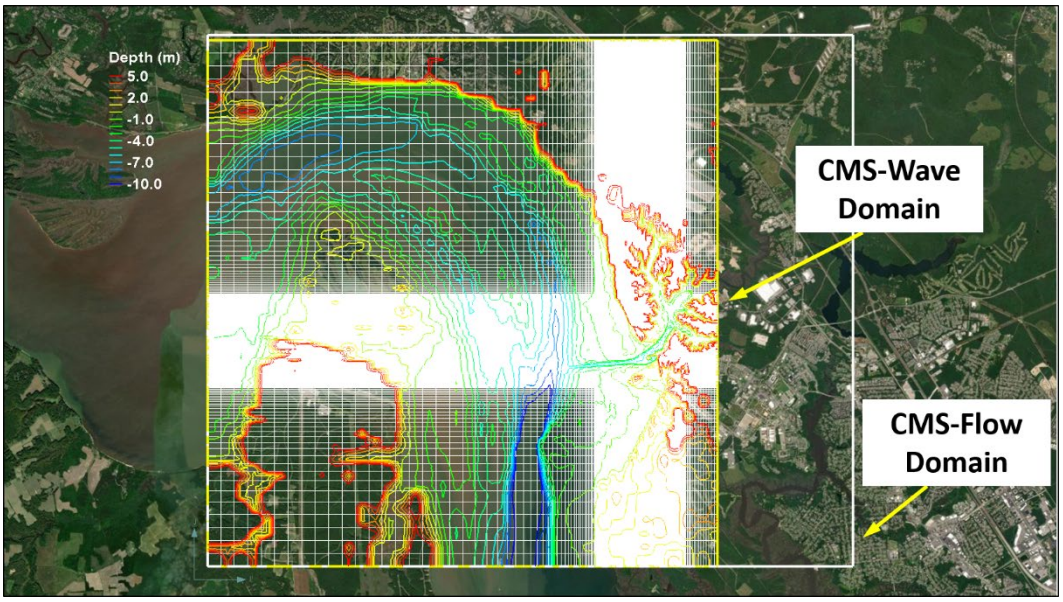

Figure 4. Non-uniform rectangular CMS-Wave grid and bathymetry. Yellow lines delineate the CMS-Wave domain and grid, and white lines the CMS-Flow domain.

For harbor protection, the original piers were modified, and a wave screen was designed with and without porosity (low porosity: 20-30% voids, high porosity: 35%-40% voids, solid structure) (Figure 5).

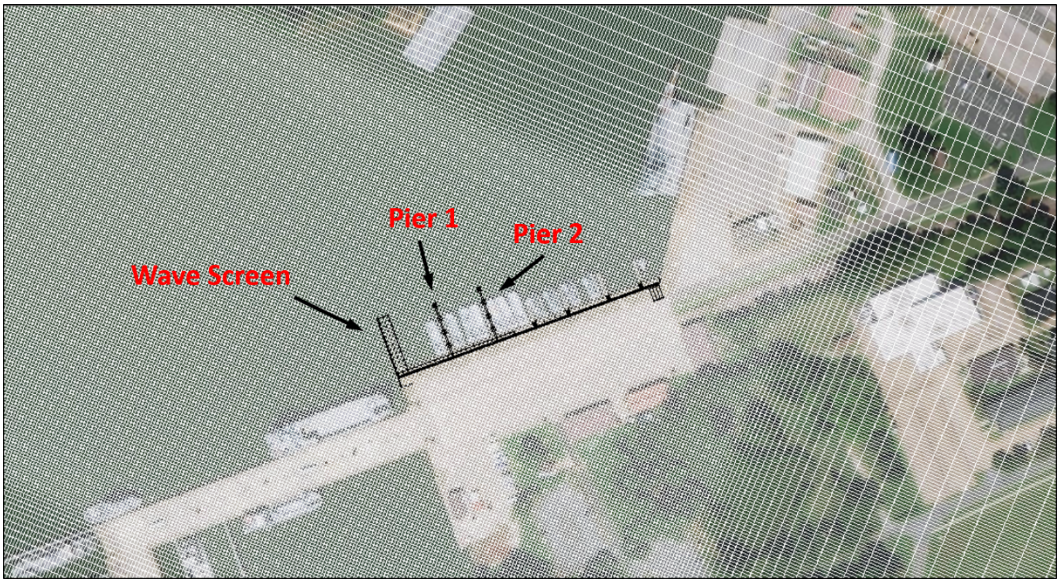

Figure 5. Location of the wave screen and modified piers at the Third Port.

To evaluate storm wave impact on the port and assess the functionality of the wave screen in reducing wave energy, a coupled wave model was configured, which included a parent and a child wave domain (Figure 6). The parent domain has a horizontal scale of 30 × 12 km with a square grid

resolution of 100 m, which provides a large fetch for waves to be developed under storm conditions. The child domain 3.0 × 1.5 km with a non-uniform rectangular grid from 2 × 2 m to 95 × 57 m.

Figure 6. Coupled CMS-Wave domains. The red polygon outlines the parent wave domain and yellow polygon the child wave domain.

2.1 Data and Model Forcing

Bathymetry and field surveys

River shorelines were delineated based on the Google Earth imagery. Bathymetry data are extracted from two datasets of the NOAA's National Centers for Environmental Information (NCEI), Coastal Digital Elevation Model (DEM) and Coastal Relief Model (CRM) (NCEIa, 2021). The first dataset has a 1/9 arc-second spatial resolution (approximately 3 m) and is applied to develop CMS model for the calculations of waves, hydrodynamics, and sediment transport; the second dataset has a 3 arc-second spatial resolution (approximately 90 m) and is downloaded to configure the coupled parent CMS-Wave model.

NAO conducted condition surveys and provided historical survey data relative to the mean sea level around the navigation channel in Skiffes Creek and James River from 2014 to 2021. The December 2014 post-dredge and the March 2016 pre-dredge survey data are shown in Figure 7. Because no dredging occurred during this period, channel depth changes were mainly affected by physical and environmental force. Therefore, the long-term (16-month) simulation was set up for this period in a way that

the post-dredge survey data collected in December 2014 were incorporated in the numerical model to configure initial model bathymetry and the pre-dredge data from March 2016 were used to examine the final model results of channel morphology change. Figure 8 shows the measured depth changes between these two surveys, which will be compared with the model calculation in the next section.

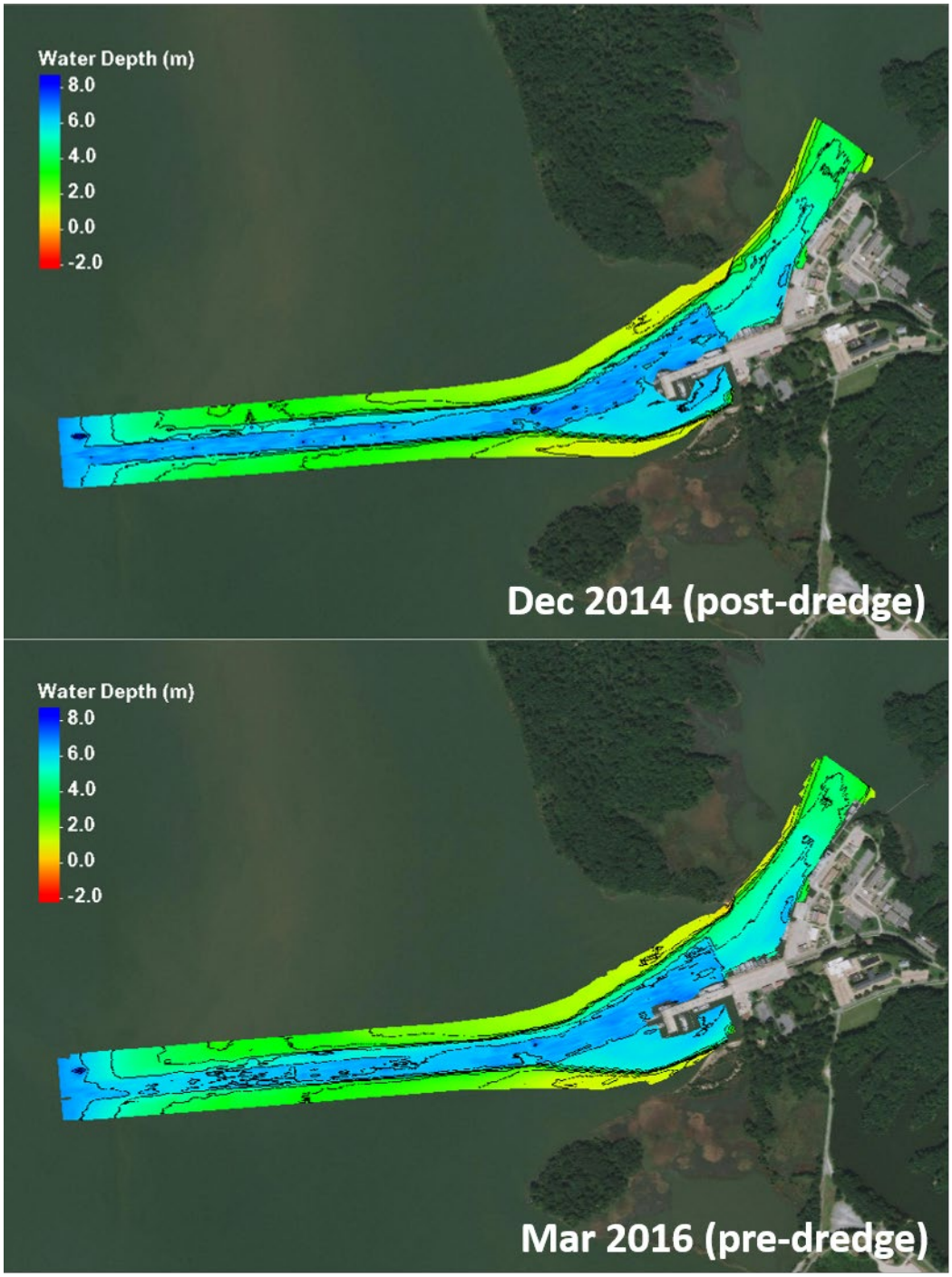

Figure 7. Channel surveys (pre- and post-dredge).

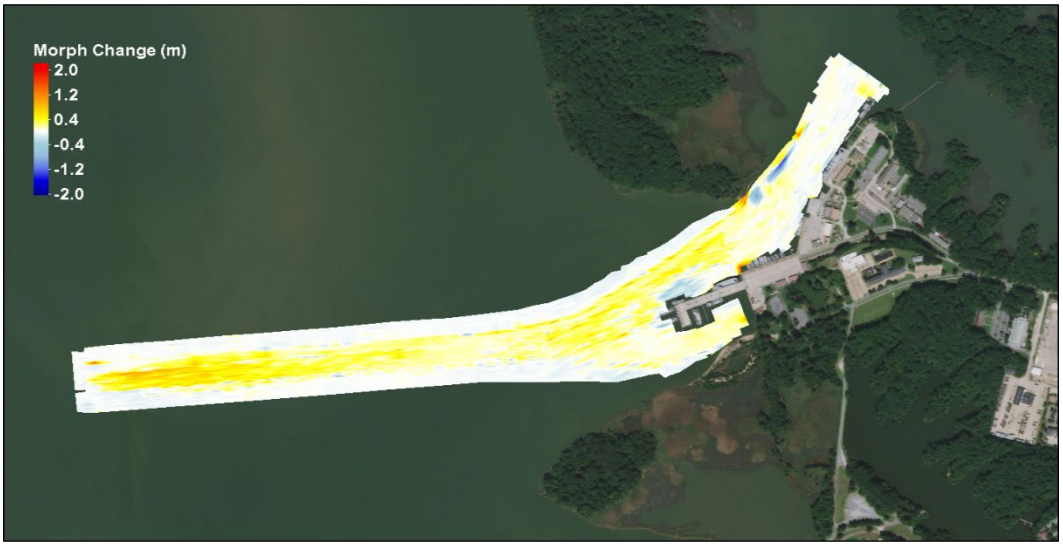

Figure 8. The depth changes along the navigation channel from December 2014 to March 2016. Bed erosion is represented by cool colors and deposition by warm colors.

Figures 9 and 10 show the 2016 post-dredge survey, the 2018 condition survey, and the 2019 and 2021 plans and specifications survey data. Similar to the channel depth changes from the 2014 to 2016 surveys, erosion occurred along the flanks of the channel adjacent to the entrance of Skiffes Creek and deposition in the middle of the channel around the west part of the survey area in James River from the 2016 post-dredge to 2018 condition surveys. Although the 2019 survey only covers the port area, comparing with the 2021 survey, clear channel infilling is still shown in front of the mooring field. The 2021 survey also went over a number of transects across the wetland area behind the port, which extends the coverage of bathymetry measurements and greatly assists the modeling analysis around the Third Port.

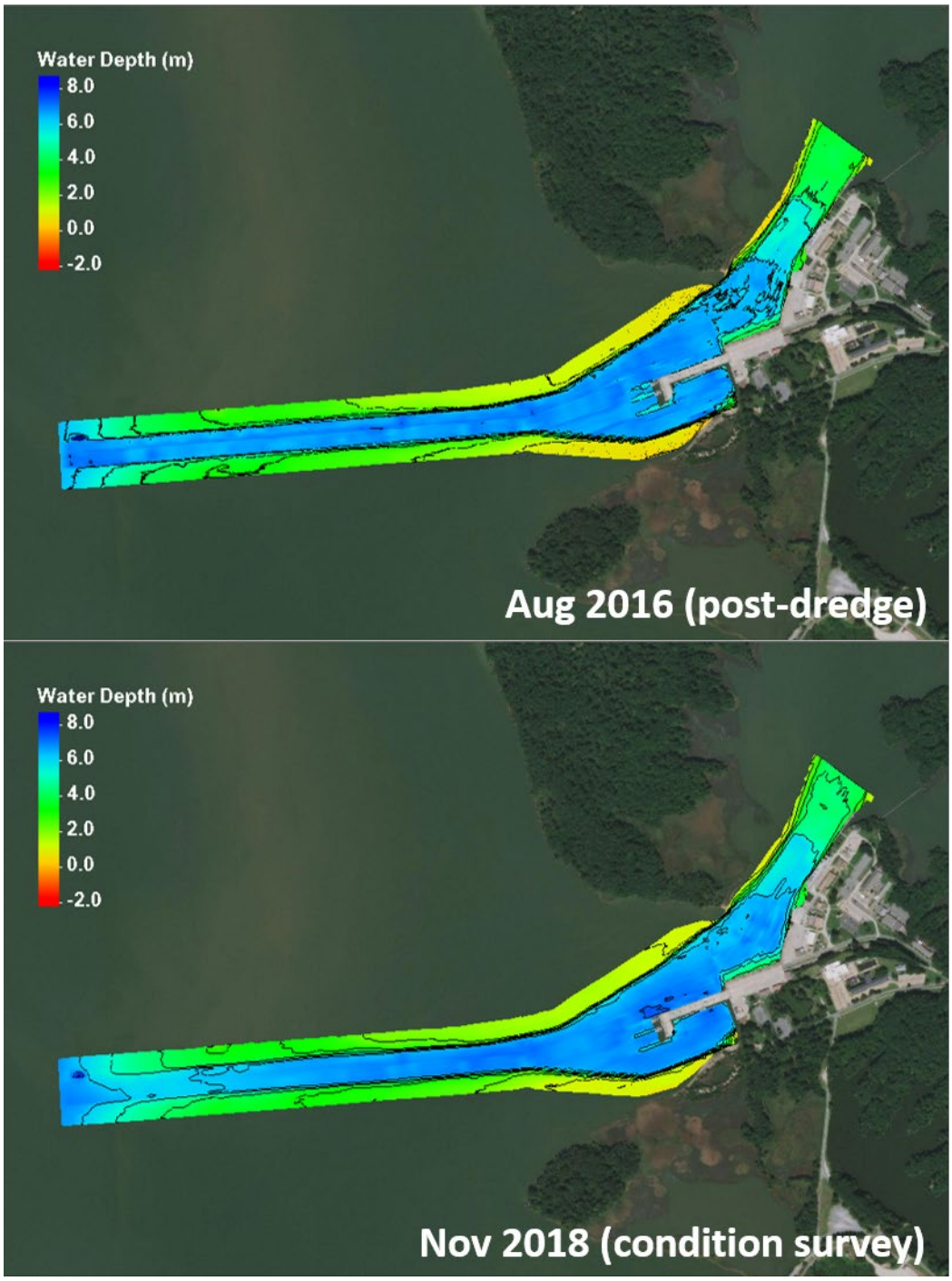

Figure 9. Channel surveys (post-dredge and condition).

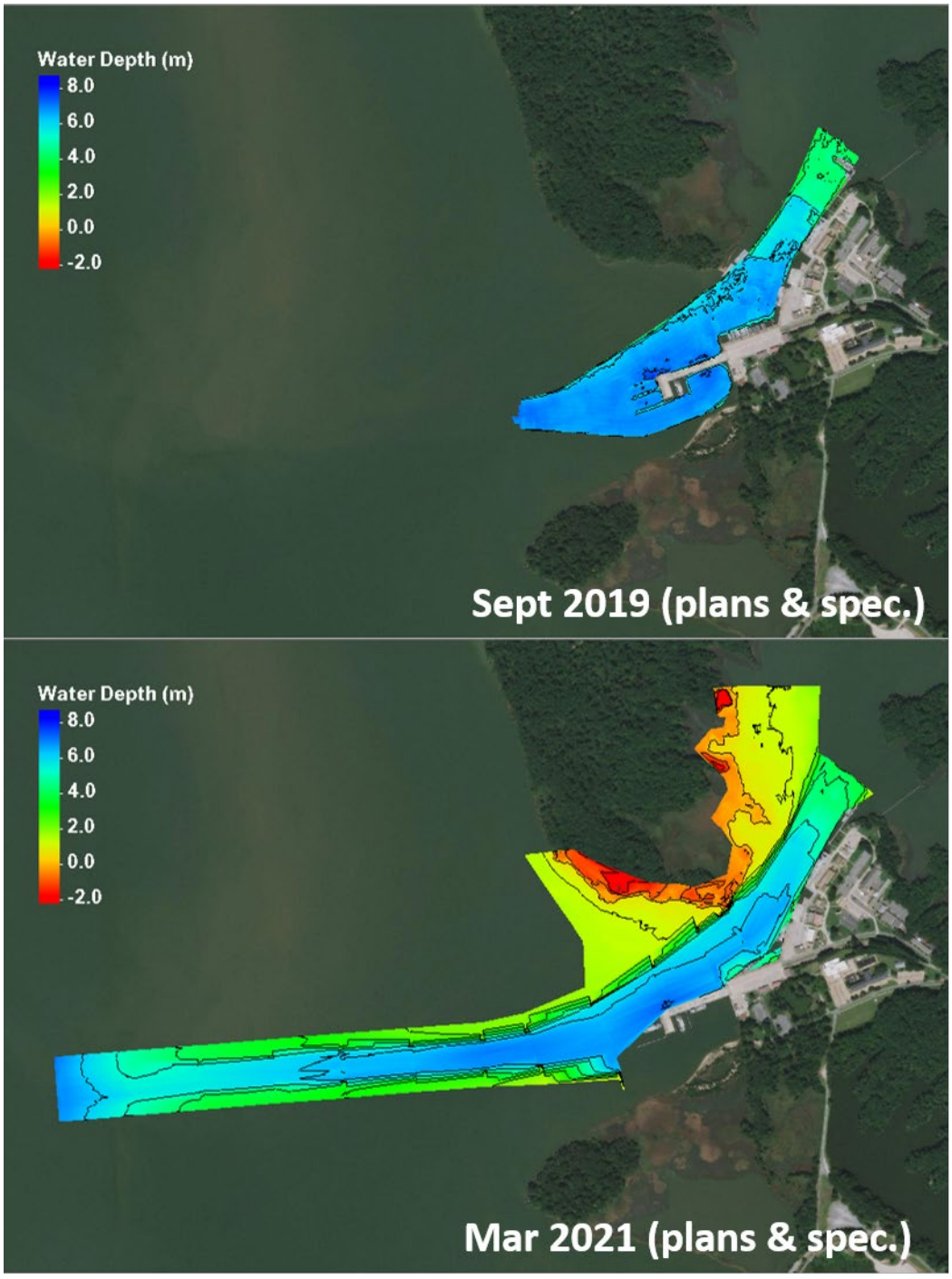

Figure 10. Channel surveys (plans and specifications).

Wind, waves, and hydrodynamics

Wave, hydrodynamic, and sediment transport simulations were conducted for a period from 1 December 2014 to 4 March, 2016. CMS-Flow was driven with time-dependent water levels and winds. Water level data were obtained from NOAA Sewells Point (8638610) at the mouth of James

River (Figure 11) (NOAA 2021). Wind data were obtained from the National Weather Service's Fort Eustis gauge (NCEIb, 2021).

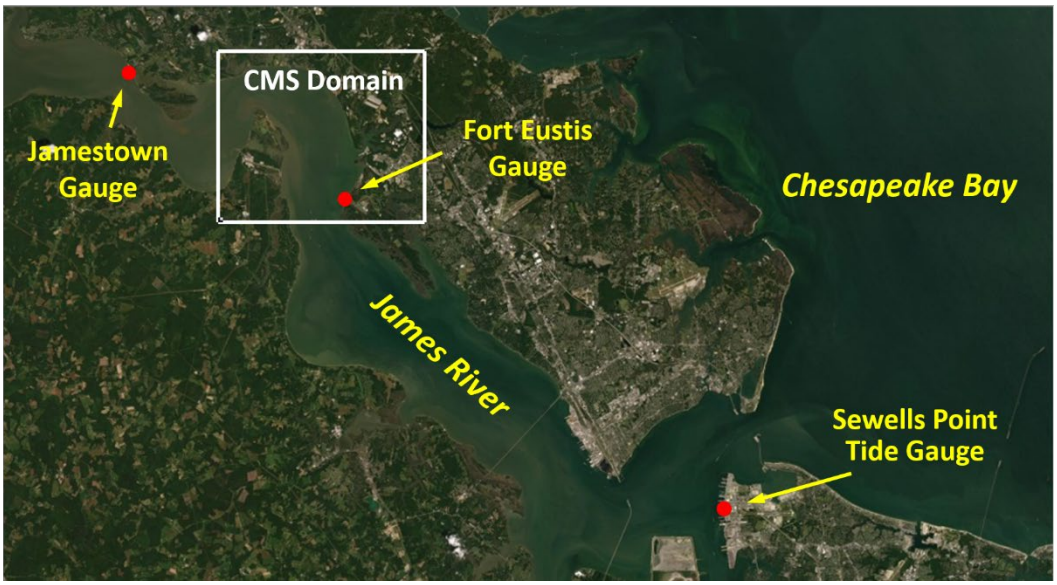

Figure 11. Locations of Sewells Point water level gauge 8638610, Fort Eustis and Jamestown gauges.

Because Sewells Point is approximately 40 km from Fort Eustis and 60 km from Jamestown, measured water levels at this location need tidal amplitude and phase adjustments before assigned to the CMS open boundaries adjacent to Fort Eustis and Jamestown. Figure 12 shows hourly water surface elevations at Sewells Point, Fort Eustis, and Jamestown gauges for the July 2010 period, which is representative of the only period when all three gauges were simultaneously operational. As the tide propagates upstream along James River, tidal amplitude is reduced and tidal phase is lagged. Based on the historical datasets, the adjusted water surface elevation at Sewells Point, as the CMS driving force, is applied at the upstream and downstream open boundaries.

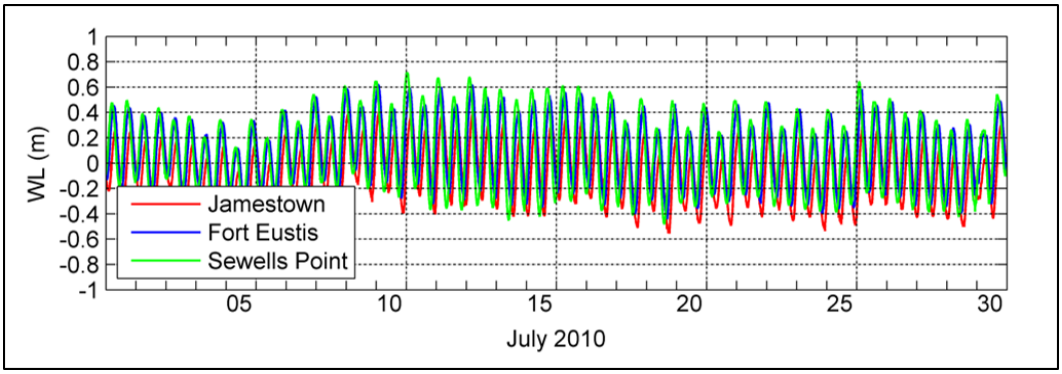

Figure 12. Water level data at of Sewells Point, Fort Eustis, and Jamestown gauges for the July 2010 period.

Figure 13 shows the wind rose for the simulation period from December 2014 to March 2016. The mean wind speed is 2.7 m/s over the 16-month period and the dominant wind direction is from north.

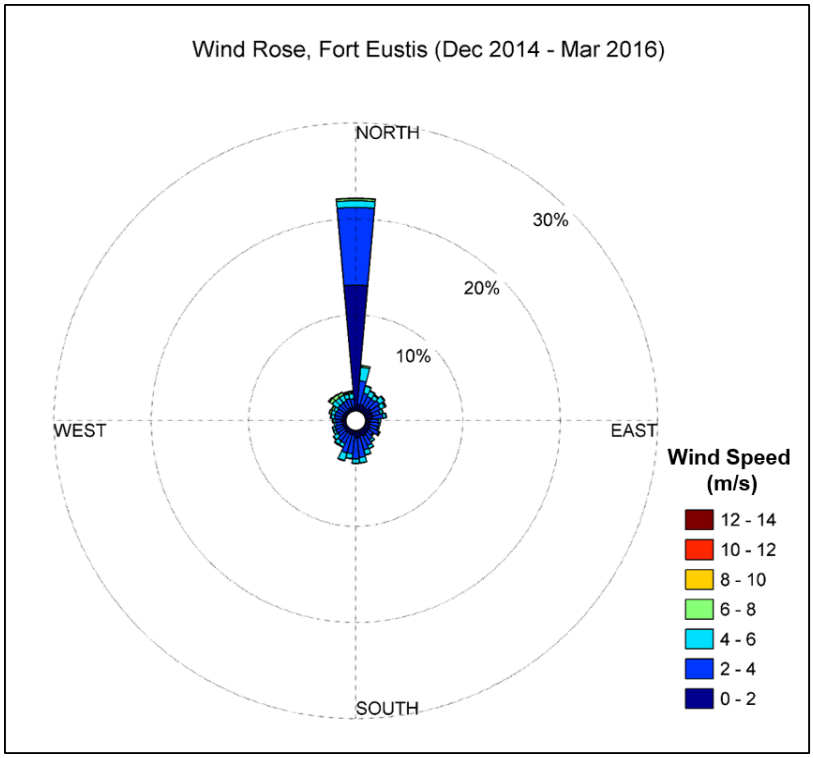

Figure 13. Wind rose at Fort Eustis gauge for the period from December 2014 to March.2016.

As the model surface boundary condition, wind force is specified at air-water interface to drive the hydrodynamics and to generate storm waves in model calculations. For the evaluation of the designed wave screen, the coupled wave model is driven by a designed storm wind speed of 47 m/s (105 knots).

2.2 Alternatives

Alternatives were developed to investigate 1) the impact of structure installation on sediment erosion and deposition patterns at the modular causeway mooring field of Third Port and 2) the reduction of wave energy by modifying and relocating existing piers and adding a wave screen at the port.

A detailed description of the alternatives is as follows:

Alternative 1: specification of a submerged riprap in the mooring pile field.

Alternative 2: specification of a submerged sheet pile bulkhead in the mooring pile field.

Alternative 3: existing pier modifications and specification of a wave screen without permeability (solid wave screen).

Alternative 4: existing pier modifications and specification of a wave screen with low permeability (20%-30% voids).

Alternative 5: existing pier modifications and specification of a wave screen with high permeability (35%-40% voids).

Figure 14 shows the sketches of designed riprap and sheet pile in front of the mooring pile field and the locations of wave screen and modified piers at the port.

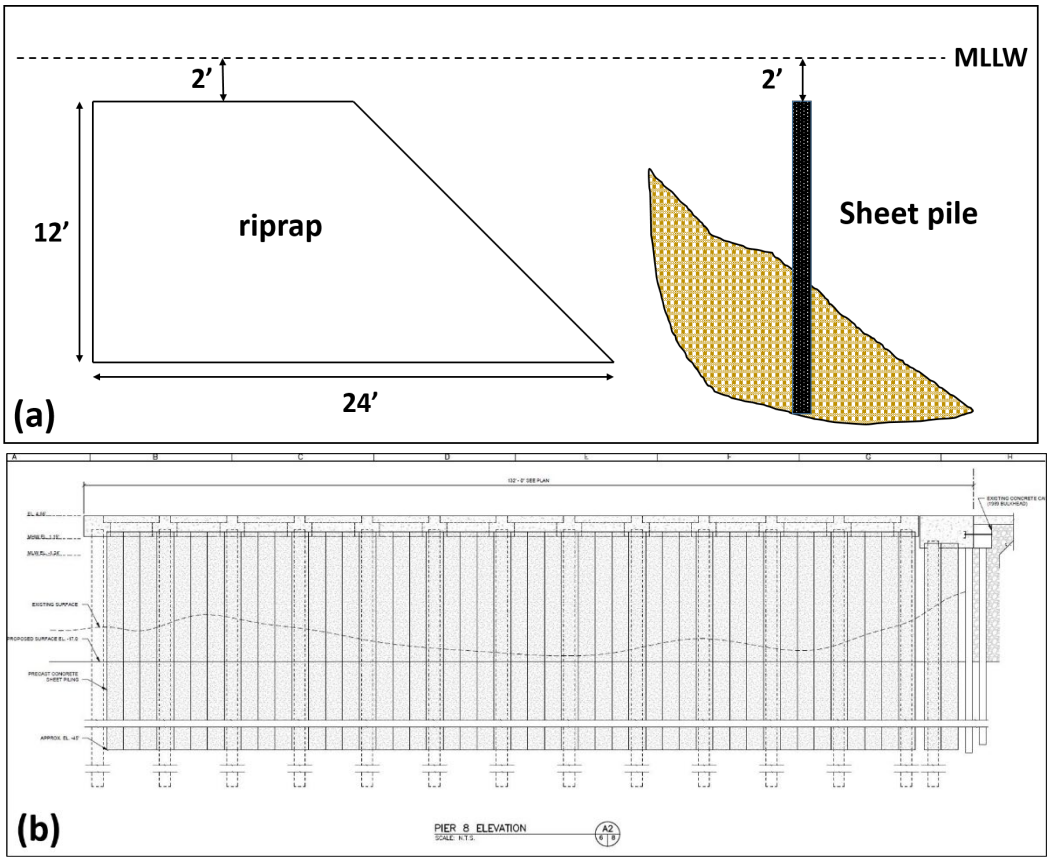

Figure 14. Design sketches of (a) the riprap and sheet pile and (b) the modified piers and wave screen at Third Port.

Model representation of the structures is shown in Figure 15. For Alternatives 1-2, model results with and without the specifications of the riprap and sheet pile structures are compared and the changes in sediment transport pattern are examined around the mooring field. For Alternatives 3-5, varying permeability of the wave screen optimizes/compares the wave forces behind it in the port.

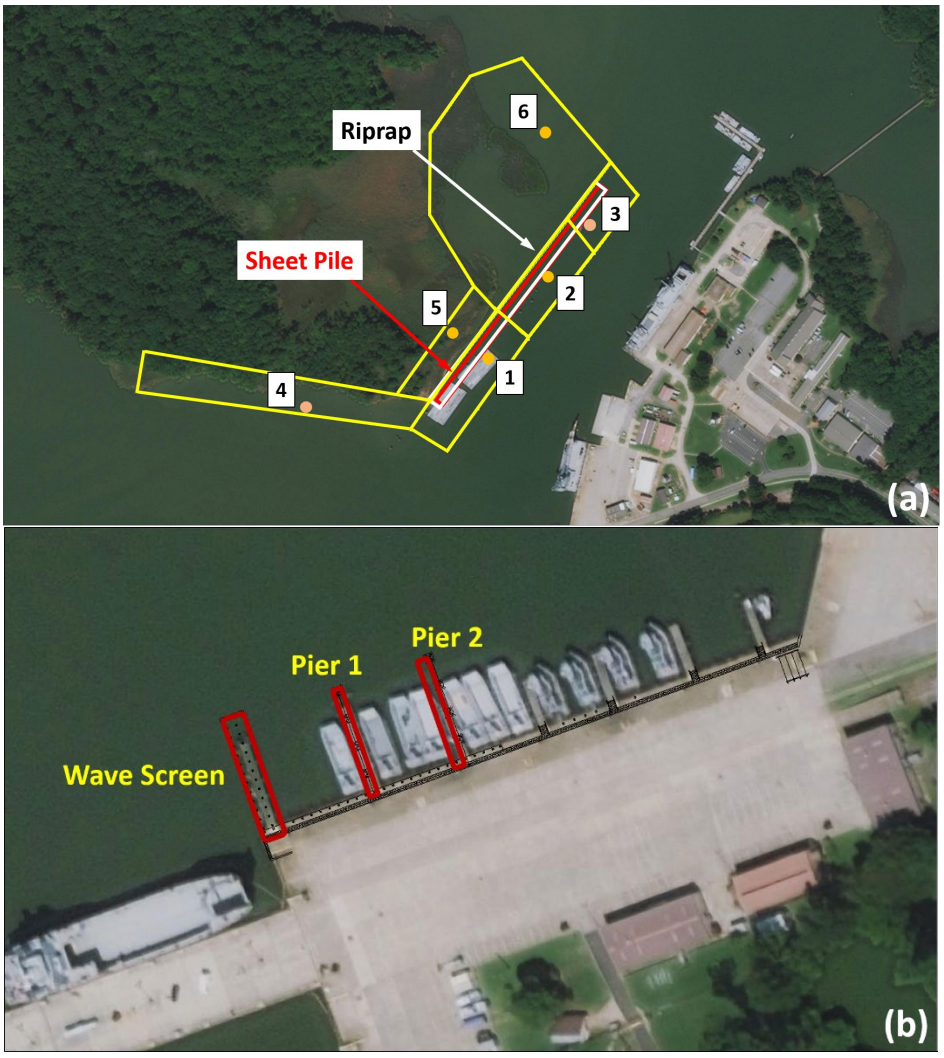

Figure 15. Specified locations of (a) the riprap (white rectangle), sheet pile (red rectangle), current speed (1-6; orange circles), and bed volume study areas (1-6; yellow outlines); (b) the modified piers and wave screen in the CMS. Yellow polygons and beige points are 6 selected areas and locations where bed volume changes and currents are compared between cases with and without structures, respectively.

3 Model Results

3.1 Current

Figure 16 shows the calculated mean depth-averaged current field at Third Port over the 16-month simulation period and during the passage of an extra-tropical storm (September 30 – October 3, 2015). The long-term averaged currents are relatively stronger in the shallow areas on the east side of the mooring field in Skiffes Creek and also on the west side at the entrance of the creek. The currents along the channel are relatively weak. The flow directions on both sides of the mooring field are towards the channel (Figure 16a).

Mean current speeds over the storm period are much larger than those long-term averages in Skiffes Creek. The storm surge inundates the wetland area behind the mooring field and the storm-induced flows go over the area from Skiffes Creek to James River (Figure 16b). Because of the overflows, average current directions are reversed comparing with the 16-month averaged currents along the shoreline on the west side of the mooring field in James River. The storm averaged flows are towards the northwest.

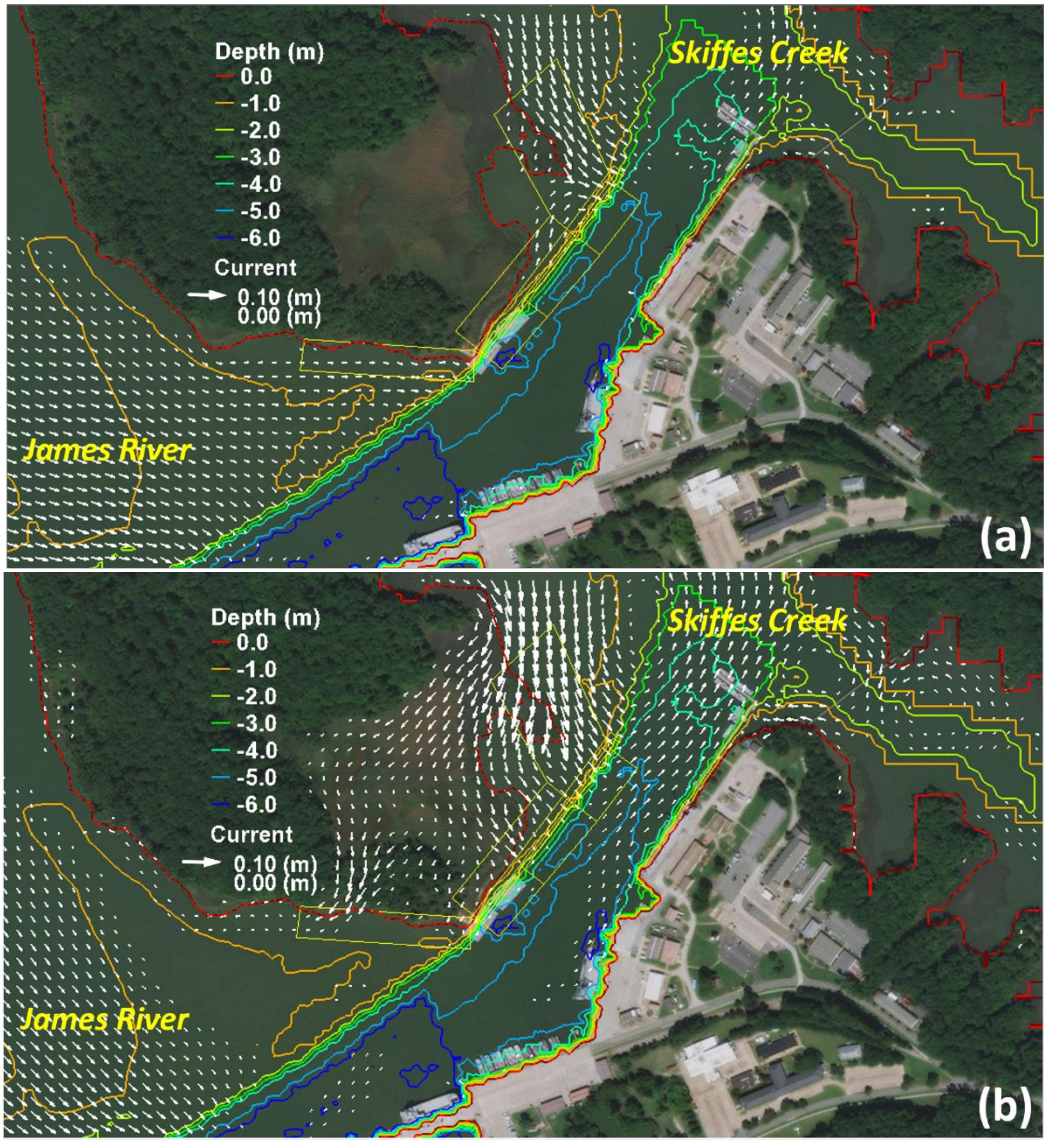

Figure 16. Calculated mean depth-averaged current field around Third Port for the period of (a) December 2014 to March 2016 and (b) during the passage of an extra-tropical storm. No structure in the mooring field.

Table 1 lists the comparisons of current speeds between the averages over the 16-month period and extra-tropical storm period at 6 selected locations (Figure 15a) around the mooring field. 5 out of 6 locations show larger current speeds for the averages over the extra-tropical storm period. Location 5 corresponds to the influence by the flows over the wetland area and Location 6 illustrates the large current speed and the speed increase comparing with the long-term averages in Skiffes Creek. On the west side of the port, as described early, the 16-month averaged flow direction is towards the channel but the storm averaged direction is away from the channel

towards the northwest. The smaller storm averaged flow speed at Location 4 distinguishes the two flow regimes in this area.

Table 1. Current speeds (m/s) averaged over the 16-month period and extra-tropical storm period at 6 selected locations around the mooring field (Figure 15a).

Average Period	Location					
	1	2	3	4	5	6
16-month	0.0003	0.0076	0.0100	0.0145	0.0004	0.0429
Extra-tropical Storm	0.0076	0.0138	0.0127	0.0008	0.0181	0.0608

To represent a riprap or sheet pile structure in the numerical model, water depth and bottom friction are adjusted based on its design and location (Figure 14). Those adjustments minimally change the flow pattern as shown in Figures 17 and 18; however, some minor changes can still be identified adjacent to the structure location.

Table 2 shows the comparisons of current speeds averaged over the extra-tropical storm period for the cases with and without structures at the 6 selected locations surrounding the mooring field. Locations 1, 2, and 3 are located in front of the structures next to the channel. Current speeds over the structures are clearly reduced there. Because of its wider design, the flow speeds over the riprap are reduced by more than 50% at Locations 1 and 2. Table 2 also shows that the current speeds are increased with the existence of the structures at Location 4. Because this location is at the back of the structures on the path of the overflow from Skiffes Creek to James River. It is possible that water setup behind the structures increases overflow speeds. This setup could be verified by the reduced current speeds at Location 5 next to the structures. Location 6 is more than 100 m away from the structures in Skiffes Creek and is under strong influence of storm induced currents. The current speeds do not show significant changes by the specifications of structures.

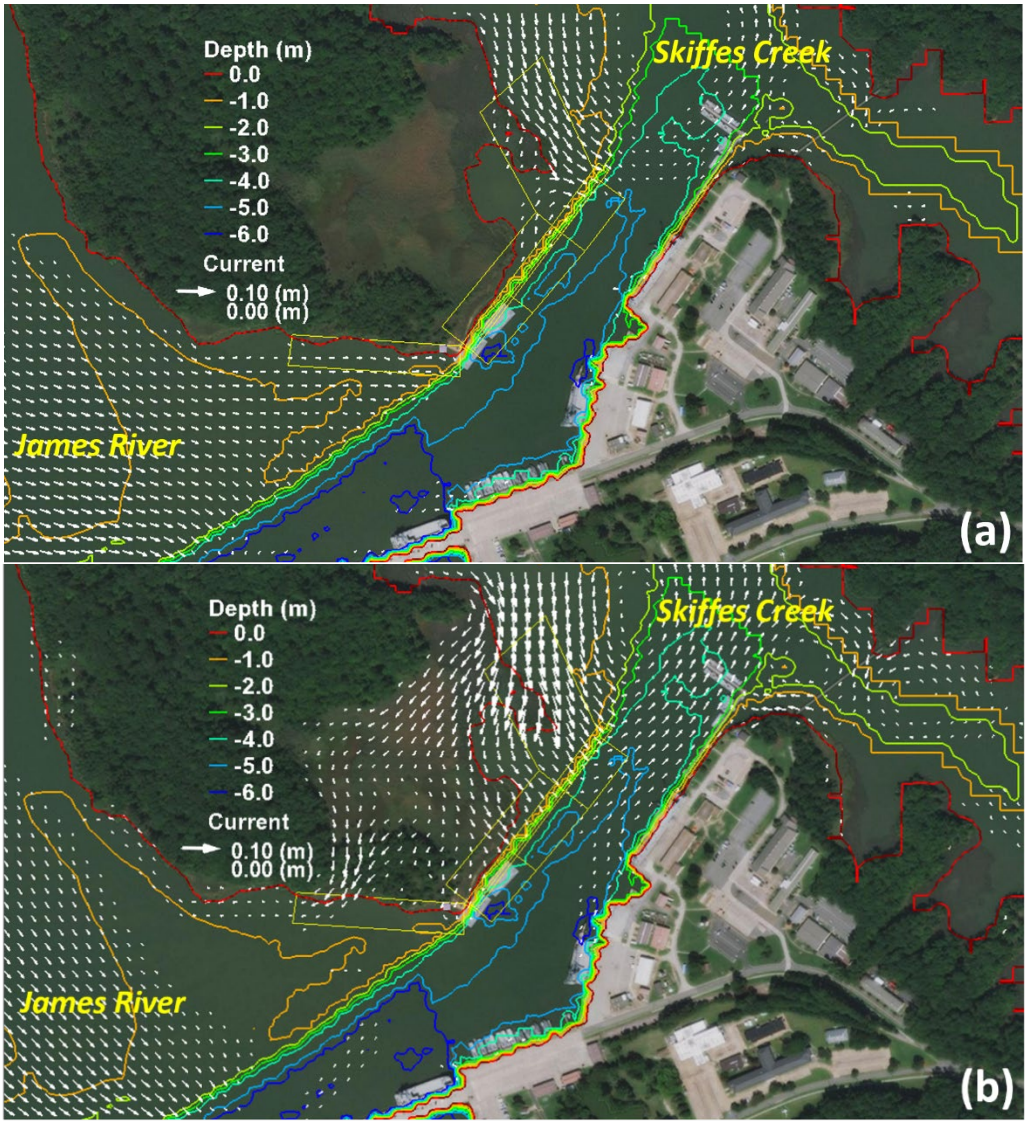

Figure 17. Calculated mean depth-averaged current field around Third Port for the period of December 2014 to March 2016. Riprap in the mooring field.

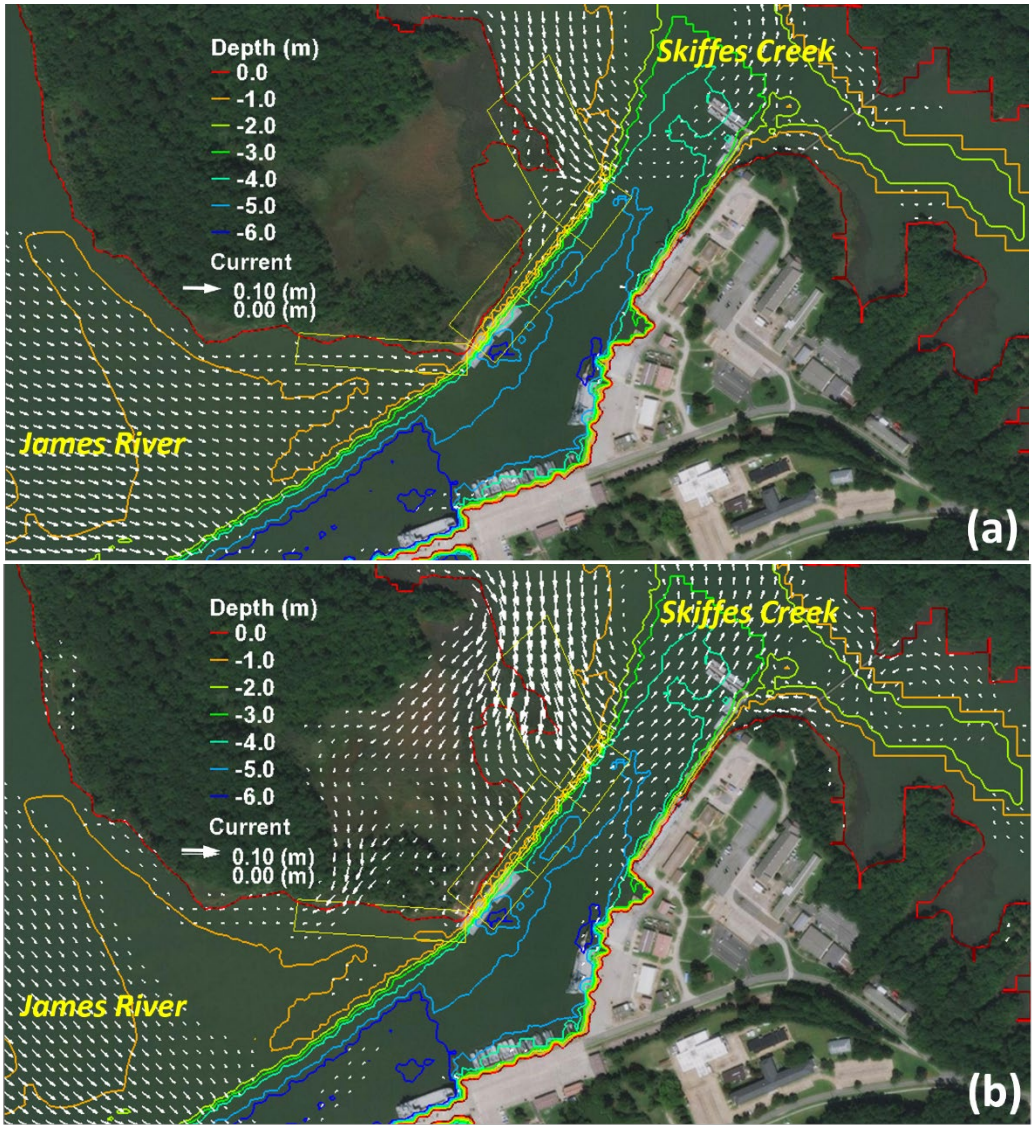

Figure 18. Calculated mean depth-averaged current field around Third Port for the period of December 2014 to March 2016. Sheet pile in the mooring field.

Table 2. Current speeds (m/s) averaged over the extra-tropical storm period for the cases with and without structures at the 6 selected locations surrounding the mooring field (Figure 15a).

Scenario	Location					
	1	2	3	4	5	6
Base	0.0076	0.0138	0.0127	0.0008	0.0181	0.0608
Riprap	0.0029	0.0060	0.0121	0.0016	0.0178	0.0602
Sheet Pile	0.0034	0.0096	0.0140	0.0028	0.0165	0.0578

3.2 Morphology and Bed Volume Changes

In general, the mean sediment transport field corresponds well to the mean current field (Li et al. 2018). Morphology and bed volume changes are determined by sediment erosion and deposition pattern associated with net sediment transport over the simulation period from December 2014 to March 2016.

The measured and calculated morphology changes in the study area are compared in Figure 19. The model results and measured data show consistent bank erosion and channel infilling patterns. The model overestimates the sediment material moving into the channel on the James River side, but the amount of sediment deposition in the channel around the port area and in Skiffes Creek shows good agreement between the survey and model results.

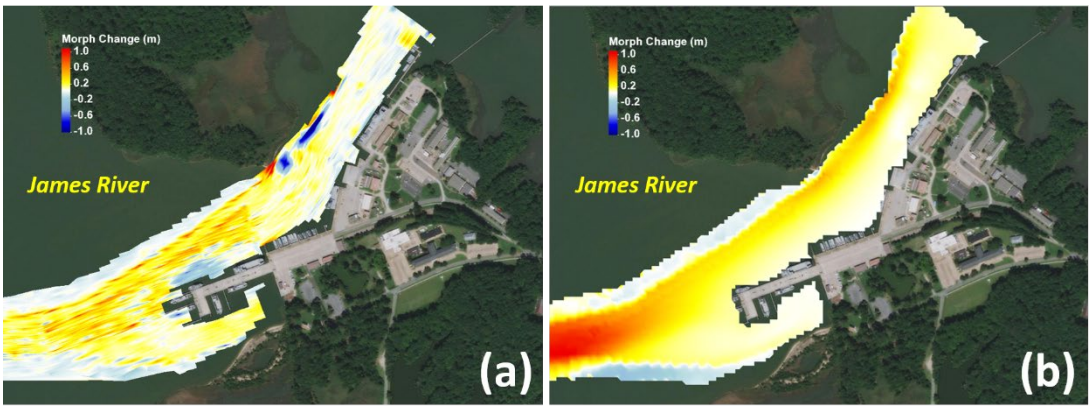

Figure 19. (a) The measured and (b) calculated morphology changes along the navigation channel from December 2014 to March 2016. Bed erosion is represented by cool colors and deposition by warm colors.

The 16-month morphology changes are shown for the base case (no structures), the riprap, and the sheet pile cases in Figures 20, 21, and 22, respectively. Differences in sediment erosion and deposition patterns can be seen on the east side of the mooring field when comparing the base case with either of the structural cases. Figures 20-22 and the mean current fields in Figures 16-18 clearly show sediment materials are eroded from Skiffes Creek and deposited in the mooring field near the channel. The contour maps of morphology changes also illustrate that more erosion/deposition around the port for the base case than the cases with the specifications of structures.

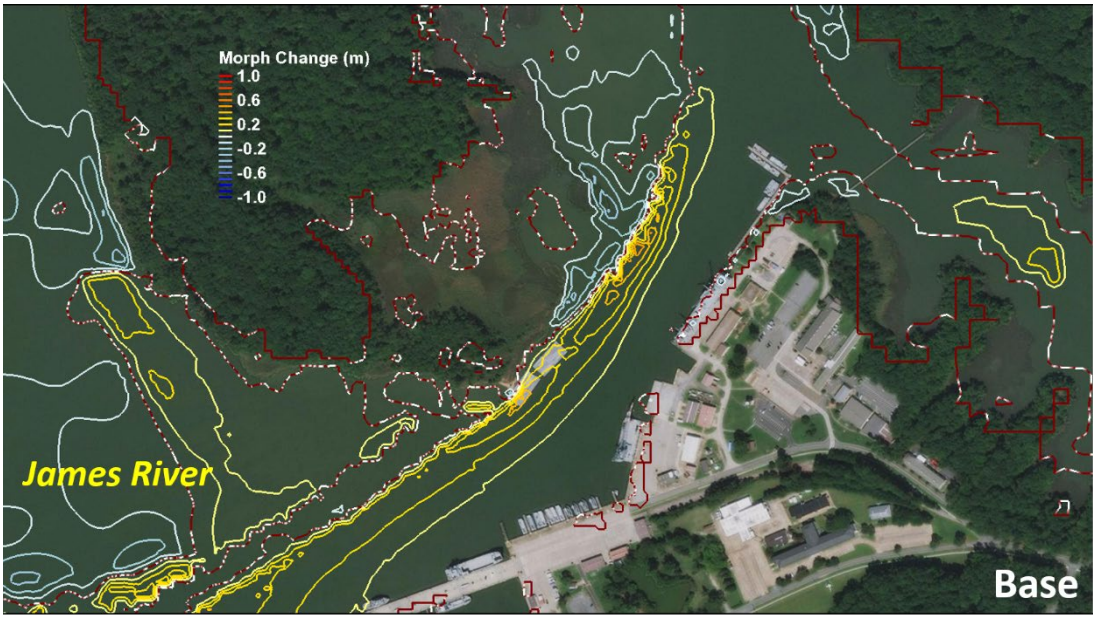

Figure 20. Calculated morphology changes without structure (base case) in the mooring field at the end of the 16-month simulation. Warmer colors represent sediment accretion and cooler colors sediment erosion.

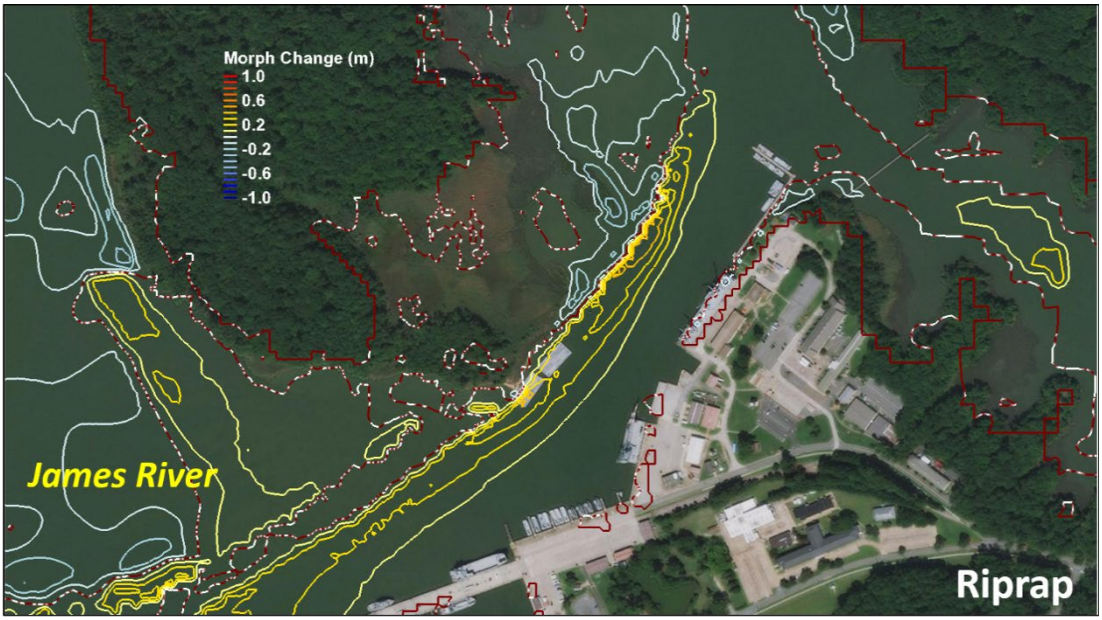

Figure 21. Calculated morphology changes with the riprap structure in the mooring field at the end of the 16-month simulation. Warmer colors represent sediment accretion and cooler colors sediment erosion.

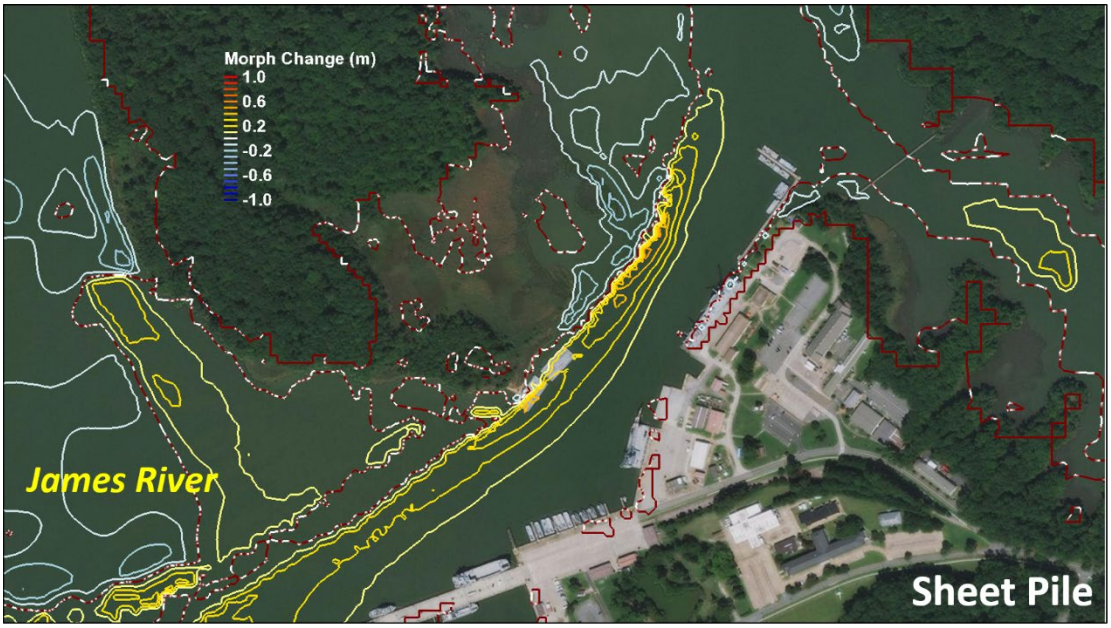

Figure 22. Calculated morphology changes with the sheet pile structure in the mooring field at the end of the 16-month simulation. Warmer colors represent sediment accretion and cooler colors sediment erosion.

Detailed comparisons of bed volume changes between the base and the structure cases are made within 6 selected areas surrounding the mooring field (Figure 15) and the values are listed in Table 3.

Table 3. Bed volume changes (m^3) between the base case and the structure cases (riprap and sheet pile structures) from December 2014 to March 2016. The negative sign indicates the volume loss and the positive the volume gain within the 6 selected areas.

Scenario	Area					
	1	2	3	4	5	6
Base	1934	1290	1051	135	-76	-3283
Riprap	1917	1643	1115	101	-59	-3081
Sheet Pile	1774	1246	1037	101	-73	-3124

Areas 1-3 are located in front of the structures, covering portion of the river channel. If, as pointed out in the previous section, the potential source of sediment input to the channel is behind the mooring field in Skiffes Creek, the volume changes in the table show that the structure specified in the model could act as a sediment barrier and reduces sediment transport and volume gain in those areas. For the riprap structure, less sediment accumulation occurs in Area 1 and for the sheet pile structure all three areas show less sediment gain. In blocking sediment transport on its way from the

creek to the channel, the sheet pile structure performs better than the riprap structure.

Areas 5 and 6 are located behind the mooring field, in which sediment erosion occurs. Table 3 shows that bed volume loss is decreased in those areas due to the specifications of structures. The decreased erosion reduces sediment supply to the downstream areas 1-3 where sediment accumulation is also consistently reduced. Referring to the analysis of the current field in the previous section, it can be seen that the construction of a structure in the mooring field could result in weaker currents and less erosion in the sediment source area, and less sediment accretion in the channel area.

Area 4 is on the west side of the mooring field and the total volume changes are small because of weak currents. With the specifications of structures, the lesser amount of volume gain corresponds to reduced current speeds behind the mooring field in the wetland area (Figures 16-18).

3.3 Evaluation of Wave Screen

Initial wave model

To evaluate the functionality of the wave screen, an initial wave grid is developed (Figure 23). Incident waves propagate from northwest with a significant wave height of 2.0 m and wave period of 4.0 seconds. Various water levels are used when running the CMS-Wave model.

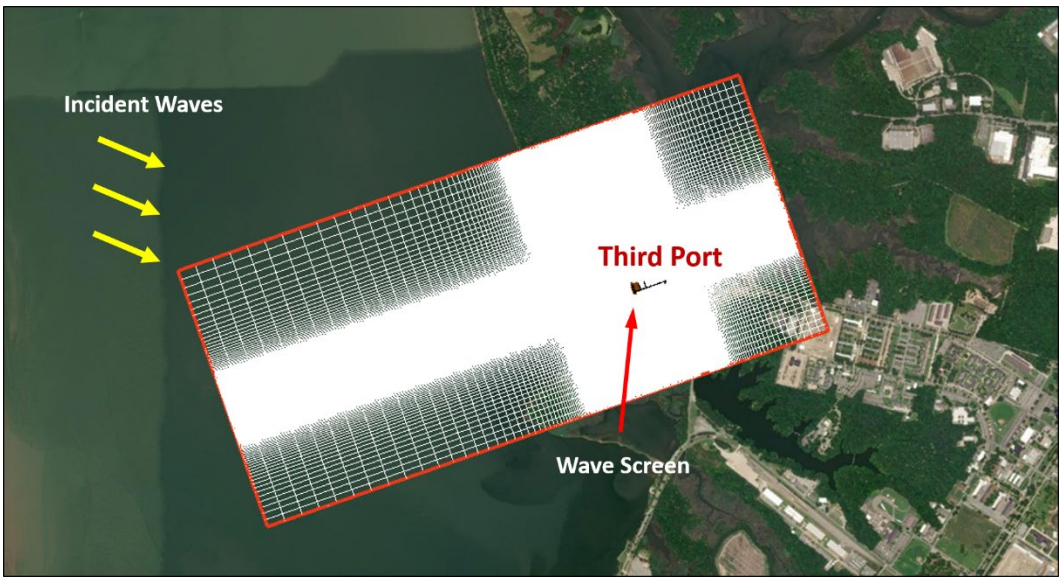

Figure 23. Initial CMS-Wave grid. Yellow arrows indicate the incident wave direction.

Table 4 shows significant wave heights obtained by spatially averaging model results along a straight line in front of the wave screen, at the back side of the wave screen, at Piers 1, and 2. For each set of incident wave conditions, solid (no porosity), low porosity, and high porosity wave screens are tested for wave transmission.

Table 4. Spatially averaged significant wave heights with various water levels in front of the wave screen, at the back side of the wave screen, at Piers 1, and 2.

Location	Water Level (m)											
	0.3			0.5			0.8			1.0		
	Wave Screen (solid)	Low Porosity	High Porosity	Wave Screen	Low Porosity	High Porosity	Wave Screen	Low Porosity	High Porosity	Wave Screen	Low Porosity	High Porosity
Front	0.404	0.419	0.415	0.498	0.517	0.513	0.626	0.647	0.643	0.765	0.785	0.785
Back	0.058	0.105	0.149	0.070	0.131	0.196	0.167	0.171	0.381	0.312	0.209	0.471
Pier 1	0.165	0.180	0.203	0.202	0.227	0.257	0.277	0.293	0.396	0.388	0.369	0.491
Pier 2	0.235	0.245	0.254	0.290	0.302	0.317	0.373	0.389	0.435	0.481	0.480	0.538

It can be seen from the table that when water level is low and total water depth is small, waves break and wave energy dissipates greatly as they approach the port. With high water level and large total water depth, significant wave heights gradually decrease in wave energy dissipation. 2 m incident waves with a specified water level of 1 m still have an average significant wave height of 0.77 to 0.79 m close to the wave screen, which almost doubles the values with a specified low water level of 0.3 m at the same location. As sketched in Figure 14, the top of the wave screen is 1.03 m above the mean sea level. Therefore, with lower water levels in the domain, wave runup and overtopping are substantially less and the wave screen functions much better than those with higher water levels.

Spatial variations in significant wave heights also show a consistent trend behind the wave screen. Right at the back side of the wave screen, significant wave heights are greatly reduced. Piers 1 and 2 are approximately 30 m and 60 m from the wave screen, respectively, where significant wave heights increase because the locations are under stronger influence of wave diffraction.

Dividing the significant wave height at the back side of the wave screen by that in front of the wave screen, wave transmission coefficients are calculated and the results are listed in Table 5.

Table 5. Spatially averaged significant wave heights in front of and at the back of the wave screen, and wave transmission coefficients through the wave screen with various water levels.

Location	Water Level (m)											
	0.3			0.5			0.8			1.0		
	Wave Screen (solid)	Low Porosity	High Porosity	Wave Screen	Low Porosity	High Porosity	Wave Screen	Low Porosity	High Porosity	Wave Screen	Low Porosity	High Porosity
Front	0.404	0.419	0.415	0.498	0.517	0.513	0.626	0.647	0.643	0.765	0.785	0.785
Back	0.058	0.105	0.149	0.070	0.131	0.196	0.167	0.171	0.381	0.312	0.209	0.471
Transmission Coefficient	0.144	0.251	0.359	0.141	0.253	0.382	0.267	0.264	0.593	0.408	0.266	0.600

With a low water level of 0.3 m or 0.5 m, no wave runup and overtopping occur. Wave transmission coefficients linearly increase from a solid to highly permeable wave screen design. With a high water level of 0.8 m or 1.0 m, wave transmission coefficients show the nonlinear increase through the wave screen due to wave runup and overtopping.

Coupled wave model

Based on the above tests, the coupled CMS-Wave simulations are set up. As shown in Figure 6, the parent grid is developed to cover a large fetch for wave development under the typical winter storm condition (wind speed: 47 m/s (105 knots)). Wave parameters are obtained from the parent wave model and assigned to drive the child wave model at its open boundary (Figure 6), which have a significant wave height of 2.06 m, a peak wave period of 4.2 s, and a dominant wave direction of 296° azimuth.

The simulations of the child wave model are conducted assuming a 1-m surge occurring adjacent to the port. Figures 24-26 show the vector field of significant wave heights corresponding to the solid, low porosity, and high porosity wave screen. The calculated results of significant wave heights and wave transmission coefficients are shown in Table 6. Similar to the analysis on Tables 4 and 5, the wave transmission coefficient is 0.468, 0.229, and 0.619 for the solid, low porosity, and high porosity wave screen,

respectively. The nonlinear increase of wave transmission coefficients through the wave screen is due to the energy redistribution between structure permeability and wave runup and overtopping.

Figure 24. Vector field of significant wave heights for the solid wave screen with a 1-m surge level around the port.

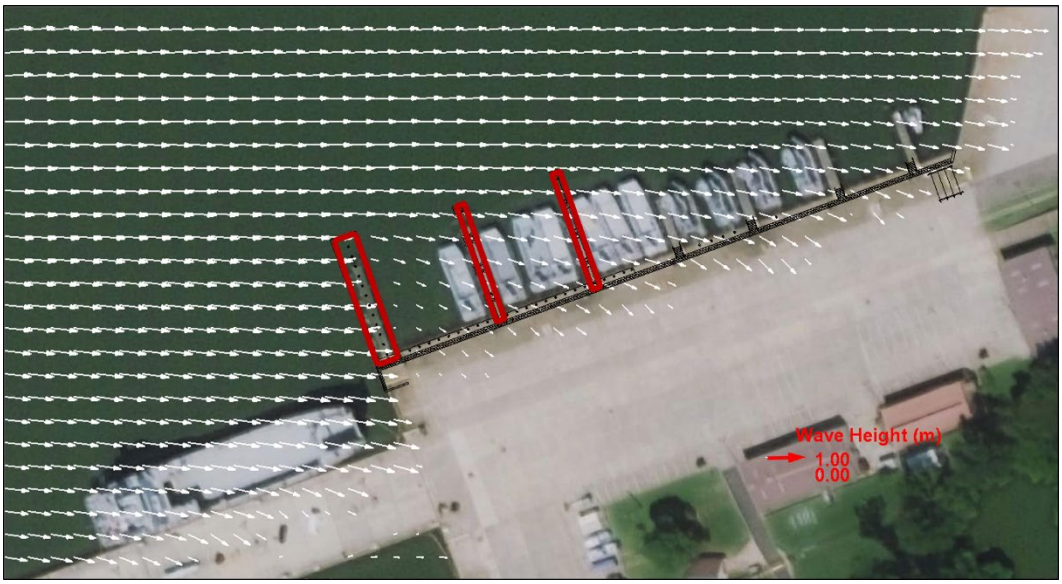

Figure 25. Vector field of significant wave heights for the low porosity wave screen with a 1-m surge level around the port.

Figure 26. Vector field of significant wave heights for the high porosity wave screen with a 1-m surge level around the port.

Table 6. Spatially averaged significant wave heights in front of and at the back of the wave screen, and wave transmission coefficients through the wave screen with a specified water level of 1 m.

Location	Wave Screen		
	Solid	Low Porosity	High Porosity
Front	0.731	0.738	0.742
Back	0.342	0.169	0.459
Transmission Coefficient	0.468	0.229	0.619

4 Summary

The Coastal Modeling System (CMS) is developed to calculate current, waves, sediment transport and morphology change around the Third Port in Skiffes Creek and James River. Driven by tide, wind, and waves, the CMS modeling include a 16-month hydrodynamic, wave, and sediment transport simulation, and multiple steady-state wave simulations. For the long-term simulations, two alternative cases are configured, in which a riprap structure and a sheet pile structure are specified in the mooring field, respectively. Current, sediment transport, and bed volume changes are investigated for the structure alternatives. For the steady-state wave simulations, the wave transmission of a wave screen with and without permeability is evaluated in the port. From this modeling application, the main points are summarized as follows:

1) Based on the averaged current fields for the 16-month and extra-tropical storm periods, the sediment transport pattern around the Third Port is obtained and the corresponding bed volume changes are analyzed. The sediment source is identified concerning the materials accreting in the mooring field and infilling the channel.

2) The calculated mean current field and bed volume changes are compared between the base case and the two structure alternative cases surrounding the mooring field. The CMS results show that both a riprap and a sheet pile structure can act as a sediment barrier in the study area. The sheet pile structure functions better than the riprap structure in blocking sediment accumulation in the mooring field (areas 1-3).

3) The identified sediment source area (area 6) behind the mooring field in Skiffes Creek shows weaker currents and less erosion when a structure is specified in the model, which also indicates less sediment supply to the mooring field and the channel area over built structures.

4) The solid and permeable wave screens are examined with varying water levels. Spatially averaged significant wave heights are greatly reduced at the back of a solid wave screen (no porosity) when a small water level is specified in the wave simulation. Farther away from the wave screen, significant wave heights are increased under the influence of wave diffraction. When a higher surge level is specified for a model simulation, wave transmission is interfered with porosity of wave screen and wave

runup and ovetopping, and transmission coefficients do not show linear increase with the increasing distance behind the wave screen as a lower water level is specified.

References

Aquaveo. 2020. Surface-water Modeling System (SMS), version 13.0, http://www.aquaveo.com/software/sms-surface-water modeling-system.

Li, H., Brown, M., Beck, T., Frey, A., Rosati, J., Habel, M., Winkelman, J., O'Donald, E., and Watts, I. 2018. "Merrimack Estuary and Newburyport Harbor Sediment Management Studies". The Technical Report ERDC/CHL TR-18-07, U.S. Army Engineer Research and Development Center, Coastal and Hydraulics Laboratory, Vicksburg, MS.

Lin, L., Z. Demirbilek, and F. Yamada. 2008. CMS-Wave: A nearshore spectral wave processes model for coastal inlets and navigation projects. Coastal and Hydraulics Laboratory Technical Report ERDC/CHL TR-08-13. Vicksburg, MS: U.S. Army Engineer Research and Development Center.

McLaren Engineering Group 2019. Fort Eustis Design Charette, Newport News, VA, Prepared for: U.S. Army Corps of Engineers – Philadelphia District, November 22, 2019.

NCEI. 2021a. National Centers for Environmental Information, Continuously Updated Digital Elevation Model (CUDEM) - 1/9 Arc-Second Resolution Bathymetric - Topographic Tiles. https://doi.org/10.25921/ds9v-ky35, accessed 14 October 2021.

NCEI. 2021b. National Centers for Environmental Information, National Oceanographic and Atmospheric Administration, https://www.ncei.noaa.gov/, accessed 14 October 2021.

NOAA. 2021. Tides and currents. National Oceanographic and Atmospheric Administration, http://tidesandcurrents.noaa.gov/, accessed 14 October 2021.OAA. 2020. Tides and currents. National Oceanographic and Atmospheric Administration, http://tidesandcurrents.noaa.gov/, accessed 30 September 2020.

Sanchez, A., W. Wu, T.M. Beck, H. Li, J. Rosati III, R. Thomas, J.D. Rosati, Z. Demirbilek, M. Brown, and C. Reed, 2011a. Verification and Validation of the Coastal Modeling System, Report 3: Hydrodynamics, ERDC/CHL Technical Report 11-10, U.S. Army Corps of Engineers Research and Development Center, Vicksburg, MS.

Sanchez, A., W. Wu, T.M. Beck, H. Li, J.D. Rosati, Z. Demirbilek, and M. Brown, 2011b. Verification and Validation of the Coastal Modeling System, Report 4: Sediment Transport and Morphology Change, ERDC/CHL Technical Report 11-10, U.S. Army Corps of Engineers Research and Development Center, Vicksburg, MS.